

1. Introduction

This readme file describes several upgrade points from the first public release version (V1.4). Validation studies of V1.4 showed that there were negative biases of the H₂O, CH₄, and O₃ data in the northern hemisphere (NH) measurements, although no major biases were found in the southern hemisphere (SH) measurements. The H₂O data in the NH especially showed exceptional profiles, thus they are not open to the public. In order to consider this problem, we have developed this new retrieval algorithm, V2.

Please be noted that before you use the ILAS-II data, you should also read a below [\[readme file of V1.4\]](#).

2. Transmittance Correction

We applied the following method to correct abnormal transmittance caused by the distortion in the entrance slit due to solar heat energy. This correction was applied only for the Northern Hemisphere data, because the transmittance distortion apparently appeared only for sunrise occultation events.

In order to correct the above we modeled the distortion in entrance slit by using the following four parameters:

1. Maximum allowable movement of Ch. 1, 2, 4's lower edge (L_{MAX})
2. Maximum allowable movement of Ch. 1, 2, 4's upper edge (U_{MAX})
3. Slit alignment offset (A)
4. Element numbers of Ch.5 used for transmittance residual calculation (R)

* Ch.1: IR channel, Ch.2: Mid-IR channel, Ch.4: Visible channel, Ch.5: Sun-Edge Sensor

Among these parameters, A was fixed to be -10 micron by the knowledge and data estimated by the laboratory experiment. These three remained parameters were determined per day basis by comparing the modeled transmittance measured by ILAS-II, and the reference transmittance calculated by using gas profiles from other satellite sensors, as follows:

Firstly, theoretical solar disk image was created for the Sun-Edge Sensor (SES) wavelength (1050 nm) using the theoretical limb darkening effect and measured aerosol extinction data at 780 nm. Also, smeared sun-edge shape, which has occurred owing to the effect of instrument function, was considered.

Secondly, ILAS-II correlative measurements were searched for other satellite sensors data; UARS/HALOE and Envisat/MIPAS. As a result, 177 matching events were picked up from MIPAS-IMK products (from April 7 to October 13, 2003) and from HALOE products (in May, 2003). By using gas mixing ratio profiles from these data products, reference transmittance spectra of the ILAS-II Ch.1 was calculated. Assuming this reference transmittance as true value, those three parameters (L_{MAX} , U_{MAX} , R) were iteratively solved to minimize the root-sum-square residuals between transmittance spectra of ILAS-II Ch.1 spectrometer's element #1-#8 and those calculated by reference ones. For the residual calculation, the altitude range between 20 and 40 km was used.

Thirdly, in order to apply the determined parameters for whole measurement period of ILAS-II (from January to October, 2003), time variations of parameters L_{MAX} , U_{MAX} are linearly interpolated into time. Time variation of parameter R was fit with a 3rd order polynomial with time. Parameters of April 7, 2003 were used for whole ILAS-II measurements before April 6, 2003. Similarly, parameters of October 13, 2003 were used for whole ILAS-II measurements after October 14, 2003.

3. Tangent height (TH) Registration

The ILAS-II Version 1.4 data have difficulty in determining the tangent height due to SES signal distortion. In ILAS-II Version 2 data, we will apply new tangent height registration method using information of the angle of the gimbal mirror instead of the combined method in Version 1.4 [Tanaka et al., 2007].

The gimbal mirror is arranged to guide incident sun light to the spectrometers and the angle of the gimbal mirror is recorded during measurements of the ILAS-II. By using the position of the satellite, the earth, and the gimbal mirror angle, we calculated the optical path of instantaneous field of view (IFOV) center, then the tangent height was derived.

The SES method applied in Version 1.4x is affected by Polar Stratospheric Clouds (PSCs) at around 20 km. On the contrary, the tangent height registration using the gimbal mirror has an advantage of being unaffected by the presence of PSCs.

4. Trend correction in 100% level signal part

Only in the sunset mode measurements, there were less measurement frames above an altitude of 80 km in the atmospheric measurement part for a lot of scenes. In addition, the 100 % level signal part was partly affected by the plastic deformation of the entrance slits, unlike for the sunrise mode measurements where the atmospheric measurement part was affected. Therefore, a conventional trend correction method for the 100 % level signal part data [Yokota et al., 2002] could not be applied for the sunset events. Instead, a brief method was developed and applied in V2; the output signal at TH of 80 km was used for the 100 % level.

5. Other revised items

5.1 Satellite position

Satellite position data were updated and the interpolation method for determining the satellite position was revised.

5.2 Abnormal data correction in the AC detection mode

The correction method, for the abnormal signal data in the AC detection mode, was revised.

5.3 Sunspot correction

In the Version 1.4 algorithm, we corrected the effects of solar limb-darkening and the sunspot existence for the aerosol extinction coefficient at 780 nm data. However, some of the data were not properly corrected. We have developed an alternative method to estimate the position of the IFOV by assuming a constant scanning speed during the scan-mode measurement.

5.4 Solar limb-darkening correction in Ch.1

The effect of solar limb-darkening in Ch.1 was calculated theoretically and corrected. This was the same as in the ILAS Version 5.2 algorithm [Yokota et al., 2002].

5.5 Refinement of the instrument function of Ch.4

The instrument function of Ch.4 was refined by using the solar line data measured by LPMA for all of the spectral ranges in Ch.4.

5.6 Ripple effect in Ch.4

There is small ripple effect in the measured signal of Ch.4, due to multiple refraction in the band-pass filter over the detectors. This effect was estimated theoretically and corrected.

5.7 Local radius of the Earth

The path-length calculation for Ch.1 and Ch.4, in the retrieval of aerosol extinction coefficients, was changed to use the local radius of the Earth in stead of a constant radius of the Earth.

5.8 Interpolation method to the layer boundary

An interpolation method of the measured signal to the layer boundary at each 1 km was revised for correcting a problem which occurred when the tangent height has not varied monotonically.

5.9 Reference Atmosphere Model (climatology)

The Reference Atmosphere Model of water vapor is updated by using the Version 3 of POAM III data.

5.10 Look-up table

The look-up table for calculating absorption cross-section data in the forward calculating procedure for Ch.1 was re-constructed by using the HITRAN 2004 database [Rothman et al., 2005].

5.11 Altitude at which the retrieval starts

The retrieval of gas profiles by the Onion-Peeling technique started at an altitude of 73 km. However, the retrieval of aerosol profiles and gas profiles in April in the Southern Hemisphere started at 71 km.

5.12 Refinement of the instrument function of Ch.1

The instrument function of Ch.1 was refined using the laboratory test data which were obtained prior to the satellite launch. Also, the effect of the cross-talk between the detector elements was changed to 5 %. In the Version 1.4 algorithm, a value of 2.5 % was incorrectly used

5.13 Systematic residuals in Ch.1

The retrieved gas profiles were re-evaluated by considering systematic residuals found in the measured transmittance spectra. Consequently, the internal error estimation was changed as described in Section 4.

5.14 Altitude range of the data products

The altitude range of the data products was changed to:
35 km for CFC12,
40 km and 50 km for N2O5, for SR and SS, respectively,
50 km and 40 km for ClONO2, for SR and SS, respectively.

5.15 Additional product in the AMES formatted data

We have calculated the vortex edge at each altitude by the Nash method [Nash et al., 1996] with the MetO (UKMO) data. The location relative to the vortex edge for each of the ILAS-II measurements was newly assigned as "inside", "outside", and "boundary" of the vortex.

6. Error estimation of the data products

6.1 Error bars

Error bars at each altitude for the retrieved parameters are presented in two classes; internal error and total error. A total error is calculated as the root sum of squares of the internal and external errors. "Internal" error and "External" error for each product are defined as follows. Further, the data format for errors has been modified and is described in the header of each data set.

a) Visible aerosol extinction (just the same as ILAS Version 5.20 algorithm)

Internal: The root sum of squares of errors originated from 100% value linear extrapolation, random errors in the data smoothing effect of the digital filter (0.5 Hz cutoff frequency), and errors in the absorption contribution by ozone Wulf band.

External: Uncertainties in the Rayleigh components caused by temperature uncertainties (± 2 K at 10 km altitude and ± 5 K at 70

km altitude are assumed).

b) IR gas products

Internal: Error calculated from the final residuals of convergence in the non-linear least squares spectral fitting. These errors were estimated from the second retrieval results after subtracting the estimated spectral biases.

External: Uncertainties in the non-gaseous component correction except for errors caused by linear interpolation are also included in the external error. In the non-gaseous component correction, standard gas profiles are assumed and used. This would cause some error. The magnitudes of these errors have been estimated from simulation by using 10 percentile profiles and 90 percentile profiles in the reference atmosphere model, by using 28 samples of the arbitrary selected ILAS-II measurement data, as the standard gas profiles. Effects from uncertainties of temperature*, which are used in the theoretical transmittance calculation, are also included.

(*the uncertainty of ± 2 K at 10 km altitude and ± 5 K at 70 km altitude are assumed).

1. Introduction

The Improved Limb Atmospheric Spectrometer-II (ILAS-II) is a solar-occultation satellite sensor for monitoring ozone and its related minor species. ILAS-II was put onboard the Japanese Advanced Earth Observing Satellite-II (ADEOS-II) "Midori-II" with four other sensors. ADEOS-II was successfully launched on December 14, 2002 from Tanegashima Island, Japan (30 N, 131 E) and was put into sun-synchronous polar orbit with equator crossing time of 10:30 a.m. The first test measurement of ILAS-II was performed on January 20, 2003. After the test measurements (until April 9), the operation phase started on April 10, 2003. Until ADEOS-II lost its function due to the solar-paddle failure which occurred on October 25, 2003, ILAS-II succeeded to capture more than 5800 vertical profiles of ozone (O₃), nitric acid (HNO₃), nitrous oxide (N₂O), methane (CH₄) and aerosol extinction coefficients (AEC) at 780 nm. This file describes overview and characteristics of the first public data products of ILAS-II with Version 1.4 data processing algorithm.

Please be noted that before you use the ILAS-II data, you should read, at least, Section 3 "Cautions on data quality for this version".

2. ILAS-II instrument and retrieval algorithm

ILAS-II consists of four spectrometers; ch.1 for measuring 6.21-11.76 micron (with a 44-spectral element detector), ch.2 for 3.0-5.7 micron (with a 22-spectral element detector), ch.3 for 12.78-12.85 micron (with a 22-spectral element detector), and ch.4 for 753-784 nm (with a 1024-spectral element detector), as well as a sun-edge sensor (SES). The instantaneous field of view (IFOV) at a tangent point has a 1.0 km width in the vertical and a 13 km (21.7 km for ch.3 and 2.0 km for ch.4) width in the horizontal direction for ch.1 and ch.2. The sampling frequency is 10 Hz. In order to derive mixing ratios of individual gas species simultaneously as a function of altitude, a nonlinear least squares method is utilized for spectral fitting, and an onion peeling method is applied to perform vertical profiling. Overview of the ILAS-II mission is described in Sasano et al. (2001).

Please be noted that the ch.2 and ch.3 data were not used in the Version 1.4 data retrieval.

The observed solar spectrum absorbed by gaseous species, is based on the Beer-Bouguer-Lambert law as the following relationship:

$$I(\nu) = I_0(\nu) \exp(-\int k(\nu) \rho ds),$$

where ν is wave number, $I(\nu)$ is the spectrum reaching the ILAS-II after passing through the atmosphere via path length s , $I_0(\nu)$ is the solar spectrum outside the atmosphere, $k(\nu)$ is an absorption cross section vector (cm²/molecule), and ρ is a number density vector of gases. Due to the strong intensity $I_0(\nu)$, atmospheric emission is negligible and ignored here.

On the other hand, the simulated (theoretical) $I(\nu)$ is drawn by a complicated procedure (Yokota et al., 2002 for the ILAS case), so that it is not described here.

The Levenberg-Marquardt technique is used for iterative nonlinear optimization of spectral fitting to derive the gas mixing ratios of each layer.

$$\chi^2 = (y_m - y'_m(x'_m))^T S^{-1} (y_m - y'_m(x'_m))$$

We consider an atmospheric layer with an index m . Let R and G be the number of detector elements ($R = 44$ in this case) and the number of unknown parameters ($G = 10$ in this case, namely, O₃, HNO₃, NO₂, N₂O, CH₄, H₂O, CFC-11, CFC-12, ClONO₂, and N₂O₅) in each layer. Using the notation x'_m as a $G \times 1$ vector expressing the unknown parameters, y_m as the $R \times 1$ observed transmittance vector, and y'_m as the theoretical transmittance for layer m , the residual index χ^2 of the spectral fitting can be expressed by using the weights, S^{-1} . For the calculation of S^{-1} , which is given as a diagonal matrix here, the inverse of the signal-to-noise ratio for each detector element is actually considered separately for DC/AC mode detections (see below).

2.1. DC/AC mode detections

The signal pick-up methods of ch.1 and ch.2 data are made alternatively with two different modes: the data taken by a direct current (DC) mode, the same as used in ILAS; and the data taken by an alternating current (AC) mode. The infrared signals from ch.1, 2, and 3 are read out in parallel from 88 pixels of the linear array detectors at a modulation frequency 30 Hz using a chopper. The outputs are amplified with a pre-amplifier, a lock-in amplifier, and an adjustable gain amplifier for each set of the pixels; and then transformed into a serial data stream. It is digitized with an A/D converter that has 14-bit resolution. The lock-in amplifier consists of a band-pass filter, a phase shifter, and a low-pass filter with a cut-off frequency of 1.0 Hz. It has a time constant of about 0.6 sec. Therefore, the infrared signals need to be deconvoluted to reproduce their original instantaneous signals. This type of signal detection is called DC mode. On the other hand, a function of AC mode detection was incorporated into the detection system, in which the detected signals are not fed into the lock-in amplifier, but directly digitized with an A/D converter to get better responses. This AC mode detection has been newly added in ILAS-II. [Table 1](#) shows a list of scenes which the data were acquired with the AC mode detection.

2.2. Altitude registration method

The original concept of this method is to use information from the upper edge of the sun and the center positions of each entrance slit (here, we define "slit A" for ch.3 and "slit B" for ch.1, 2, and 4) which determines the IFOV. The information will be obtained by the SES data. Owing to the abnormal SES data on orbit (see Nakajima et al. 2005, and Tanaka et al. 2007), we do not use the SES method (SES-M) as planned before the launch by now.

Nevertheless, we have developed an alternative way to use the SES data above 30 km. The basic concept behind this method is to use information from the lower edge of the sun and the center position of the slit B. Although the center position of the slit B was determined from data where both of the upper and lower edges of the slit were detectable, a combination of this SES method and the TS-M is used for this Version 1.4 data as a hybrid method, hybrid-M, (see Nakajima et al., 2002). Since we use information from the lower edge of the sun, the SES-M does not work occasionally and properly below 30 km.

Therefore, the transmittance spectrum method (TS-M) is used (see Nakajima et al., 2002) for altitudes below 30 km. The basic concept behind this method is to use the area of transmittance at some spectral element range in the O₂ A band absorption. For theoretical transmittance calculations of the O₂ A band, the United Kingdom Meteorological Office (UKMO) temperature and pressure data are used.

In summary, we use the hybrid-M above 30 km and the TS-M below 30 km.

The ch.3 data has not been used in the retrieval of data because of its bad signal to noise ratio. Therefore, the position of the slit A was not needed to be determined, and it has not been determined.

2.3. Smoothing filter and vertical resolution

A smoothing filter used in Version 5.20 ILAS data (see Yokota et al., 2002) is also used for both of the ch.1, ch.4, and SES data. A finite impulse response low-pass filter with a 0.5 Hz cutoff frequency is applied. It is applied to 21 major frame data points of level 1 data. For this Version 1.4 data, the smoothing filters were applied both to the DC/AC mode data, but such a wide filter may not be needed for the AC mode to improve vertical resolutions (under considerations).

The corresponding vertical resolutions (FWHM) were estimated to be 1.3 km at tangent altitude of 15 km, 1.6 km at 20 km, 1.9 km at 25 km, 2.2 km at 30 km, 2.7 km at 40 km, and 2.9 km at 50 km.

2.4. Non-gaseous contribution correction and bias error due to the aerosol/PSC presence

The non-gaseous contribution correction used in Version 5.20 ILAS data (see Yokota et al., 2002) is used for the ch.1 data. To determine the non-gaseous component in the theoretical calculation of the total (gaseous + non-gaseous) transmittance, we calculate the non-gaseous extinction coefficients at these four spectral elements, where the absorption due to gaseous species is relatively small (so-called 'window spectral element'). To do this, we used climatological values of gas VMR profiles (reference atmosphere model) as shown in Yokota et al. (2006) for calculating the gaseous contribution at these four spectral elements. The difference between the calculated (gaseous) and observed (gaseous + non-gaseous) transmittances at the four spectral elements thus gives the non-gaseous extinction coefficients by using the path length information. Finally, the non-gaseous extinction coefficients at all the other 40 spectral elements can be derived by linear interpolation between these four window spectral elements, resulting in the non-gaseous transmittance. Use of data from this reference atmosphere model would introduce some errors in the calculated transmittance at the four spectral elements, and are considered as the external error (see 2.8. Error values).

Besides the above external error, systematic (bias) errors would occur in this procedure (Yokota et al., 2002). To evaluate the systematic errors caused by the simple linear interpolation between the window spectral elements, we simulated transmittances using several types of infrared absorption spectra for the polar stratospheric clouds (PSC) such as sulfate and ternary aerosols, nitric acid trihydrate (NAT), and ice as the non-gaseous component and the above mentioned climatological profiles (a priori) as the gaseous component. By using these simulated transmittances, retrievals of the vertical profile of the gas concentration were made after applying the linear interpolation method. The difference between a priori and the retrieved gas concentration corresponds to the systematic bias error. It was also well correlated with the AEC@780 nm value, so that we evaluate the bias error as a function of the AEC@780 nm for user's convenience. See [Figure 1](#), same manner as in Figure 7 of Yokota et al. (2002).

2.5. Spectroscopic data

The HITRAN 2000 molecular spectroscopic database is used for the radiative transfer forward model calculations. For gaseous species of ClONO₂, N₂O₅, CFC-11, and CFC-12, we used the pseudo-line parameters provided by Geoffrey C. Toon of NASA/JPL. For continuum calculation of H₂O and O₂, we followed the methods of LBLRTM Ver. 8.

2.6. Temperature and pressure profiles for inputs to the forward model calculations

Originally, we planned to use T/p profiles retrieved from ch.4 data. However, further, these data have not been retrieved accurately at present, so that the UKMO daily stratospheric analyses data are used as input. At higher altitudes for which the UKMO data are not provided, we used the climatological data set of CIRA86.

2.7. Sunspot correction and solar limb-darkening correction

Originally, we planned to use a method for correcting the solar limb-darkening and the effect of sunspot existence in the IFOV using the sun scanning data which is taken at high altitudes without atmospheric absorption. The radiance distributions of the Sun are measured by this mode. However, this mode does not work very well in the ch.1 and ch.2 data, which would produce asymmetric images in the radiance distributions. Therefore, these corrections have not been performed for the ch.1 and ch.2 data so far. Since the sun scanning images in ch.4 were symmetric as expected, we could correct the effects of solar limb-darkening and the sunspot existence for the aerosol extinction coefficient at 780 nm data except for altitudes above 25-30 km (see section 3.1.4.).

2.8. Error values

The error values are provided as 'total' error and 'repeatability' error. The total error is a root-sum-square of repeatability error and 'external' error. The repeatability error refers to the random error (precision) which ILAS-II instrument itself has. It was

estimated from the repeatability of the measurements for each species (Yokota et al., 2006). The external error for gaseous species refers to errors associated with the calculation of simulated transmittance through uncertainties (that we assume arbitrary) in the non-gaseous contribution correction and temperature profiles, which are used as inputs for the retrieval. The external error for AEC@780 nm refers to error associated with Rayleigh scattering calculation through uncertainties (that we assume arbitrary) in temperature profiles. (see Yokota et al., 2002)

The repeatability (relative value) is estimated from the minimum of the relative standard deviation (1σ s.d. divided by mean) of retrieved values of each gas for each altitude. The minimum value (i.e., the repeatability condition) can be searched from each measurement period bin (roughly 7 to 8 days, consecutive 100 scenes) that is chosen every 50 scenes from April through October 2003. At altitudes where the mean value is negative, the repeatability at the closest altitude is used for this procedure.

Practically, if the repeatability multiplied by the retrieved value is smaller than the minimum of the 1σ s.d. value, the latter is used as the repeatability error. If the retrieved value itself is negative, the absolute value of that is also considered for this procedure.

[Figure 2](#) shows median value profiles of the relative repeatability error and total error for all of sunrise scenes and all of sunset scenes separately for each species.

3. Cautions on data quality for these versions.

3.1. The entrance slit of the telescope is undergone thermal deformation due to solar radiation, which we did not predict before the launch. This instrumental problem makes several data abnormal.

3.1.1. The SES data have several problems as mentioned in section 2.2. We use the transmittance spectrum method (TS-M) to determine the tangent altitude below 30 km and the SES-M above 30 km. In relation to this method, there is a small gap between altitudes registered by the TS-M and by the SES-M.

3.1.2. The measured transmittances for ch.1 and ch.2 are partially distorted, producing unreasonable shapes of vertical profiles for several species, especially for CH₄ data at altitudes above about 35-40 km.

3.1.3. The sun scanning data for ch.1 and ch.2 have not yet been utilized for correcting the effect of sunspot existence and the solar limb-darkening.

3.1.4. The effects of solar limb-darkening and sunspot existence to AEC at 780 nm data are considered but it seems not working well for altitudes above 25-30 km.

3.2. We do not exclude data that may be affected by sunspots. For your reference, lists of scenes when the sunspots seem to exist in the respective (ch.1 and ch.4) IFOV are provided in [Table 2](#).

3.3. Note that the Antarctic PSC cases, gas profiles could be affected by bias errors due to the presence of PSCs (see [Figure 1](#) and section 2.4).

3.4. For the sunset measurements during April 2 and April 22, 2003, the atmospheric measurement part above 40-65 km, depending on scenes, was not recorded owing to a mistake in one of the setup commands to start measurements.

3.5. The determined altitudes in this version has a positive bias up to approximately 100 m, because the range of spectral elements used in the ch.4 data was mistakenly set up. This fact was recently found out, so that we could not consider it in this version 1.4 data processing.

4. Products to be provided

4.1. Chemical species

- i) O₃, HNO₃, N₂O, and CH₄ are retrieved from ch.1.
- ii) AEC at 780 nm are retrieved from ch.4.

4.2. UKMO data

The UKMO temperature, pressure, potential temperature, and potential vorticity data, co-located to each ILAS-II measurement, are also provided. The UKMO data are regularly supplied by Richard Swinbank of the UKMO.

4.3. UKMO + CIRA data used for the forward model calculation

The air number density profile calculated from the temperature and pressure data merged from UKMO and CIRA data are supplied as a file with the extension of *.air. Users use these files to convert from the mixing ratio data to the number density data.

4.4. Measurement location data

Latitude and longitude information at each tangent altitude and the direction of the line of sight are supplied as a file with the extension of *.mld.

5. Summary of validation for each species

5.1. Ozone (O₃) from Sugita et al. (2006)

+/- 10% for sunrise mode (northern hemisphere) between 10 and 40 km, and -30% for 50-70 km.

+/-10% for sunset mode (southern hemisphere) between 10 and 70 km.

5.2. Nitric Acid (HNO₃) from Irie et al. (2006)

-13 to +26% for sunrise and sunset modes between 15 and 25 km.

5.3. Aerosol extinction coefficient at 780 nm (AEC@780nm) from Saitoh et al. (2006)

+/- 10-15% below 20 km and -10/-30% above 20 km for sunrise mode.

-12/-66% from 20 to 25 km for sunset mode.

5.4. Nitrous oxide (N₂O) and Methane (CH₄) from Ejiri et al. (2006)

N₂O : +/- 20% or -10 to -30 % for 17-30 km for sunrise mode and 13-21 km for sunset mode, small above 30km due to the signal distortion.

CH₄ : +/-5% for sunrise mode and +9% for sunset mode, exceptionally small above 25 km due to the signal distortion.

Table 1. A list of the AC mode measurements.

Observation Date	Occultation event ID
12 February 2003	20030212530
20 March 2003	20030320540
	20030320550
14 - 28 May 2003	20030514310 - 20030528011
16 July 2003 - 24 October 2003	20030716160 - 20031024280

Table 2. Suspicious date (yyyymmdd) that the species data could be affected by the presence of the sunspots. Asterisk shows larger sunspots occurred. Consequently, the CH₄ data (not provided), for instance, seem to be abnormal for altitudes above 30 km or so.

ch.1 sunrise	ch.1 sunset	ch.4 sunrise	ch.4 sunset
20030429	20030429	20030402	20030403
20030430	20030430	20030404	20030412
20030501	20030501	20030410	20030415
20030502	20030607	20030413	20030417
20030607	20030608	20030415	20030428
20030608	20030610	20030416	20030429
20030609	20030611	20030423	20030430
20030610	20030612	20030424	20030501
20030611	20030613	20030426	20030514
20030612	20030702	20030427	20030516
20030613	20030703	20030429	20030524
20030702	20030704	20030430	20030527
20030703	20030806	20030502	20030602
20030704	20030807	20030507	20030607
20030705	20030808	20030515	20030609
20030805	20030813	20030520	20030610
20030806	20030814	20030524	20030612
20030807	20030924	20030525	20030618
20030808	20030925	20030602	20030621
20030813	20030926	20030609	20030623
20030814	20030927	20030611	20030628
20030924	20031022 *	20030619	20030701
20030925	20031023 *	20030621	20030703
20030926	20031024 *	20030624	20030704
20030927		20030628	20030705
20031022 *		20030701	20030706
20031023 *		20030705	20030711
20031024 *		20030706	20030715
		20030710	20030716
		20030711	20030718
		20030718	20030720
		20030720	20030721
		20030722	20030730
		20030730	20030731
		20030802	20030802

		20030804	20030807
		20030809	20030810
		20030814	20030816
		20030815	20030822
		20030818	20030828
		20030822	20030830
		20030827	20030903
		20030902	20030906
		20030917	20030909
		20030926	20030910
		20030927	20030920
		20031001	20030926
		20031005	20030927
		20031006	20030928
		20031007	20031002
		20031014	20031005
		20031021	20031006
		20031022 *	20031012
		20031023 *	20031014
			20031021
			20031023 *

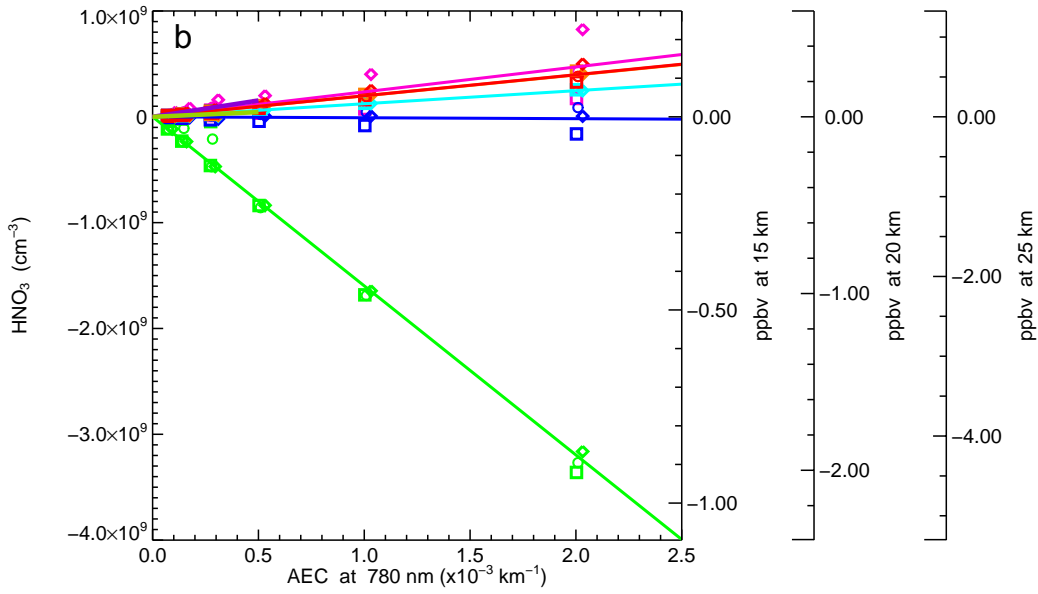
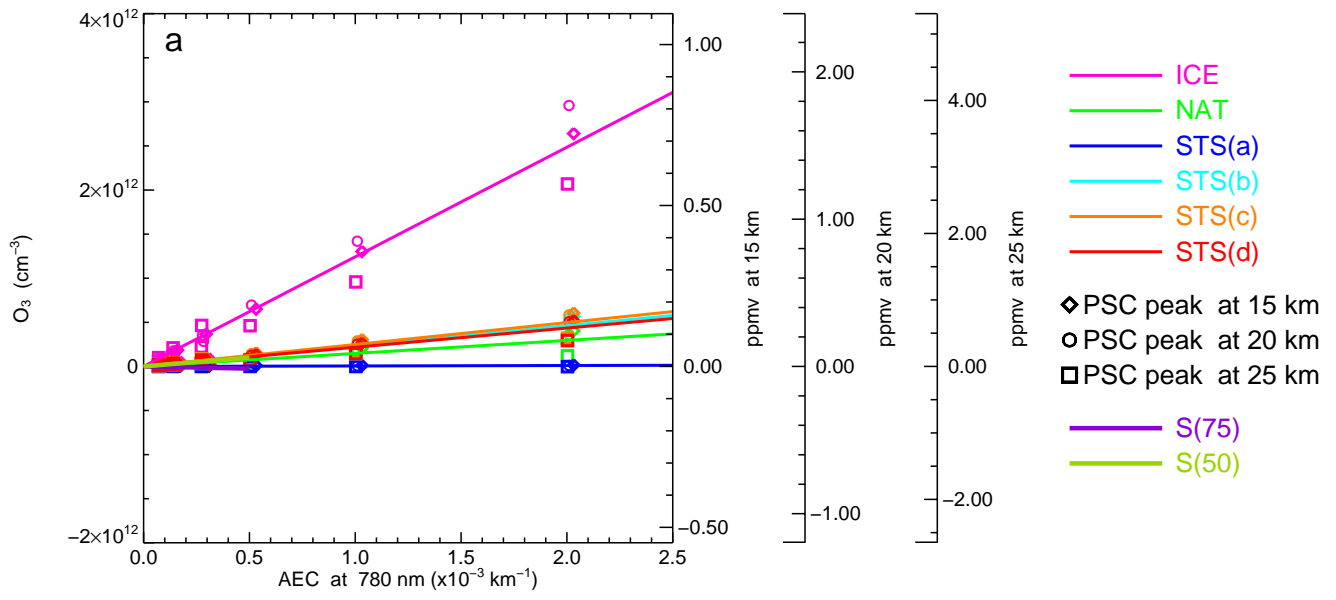


Figure 1

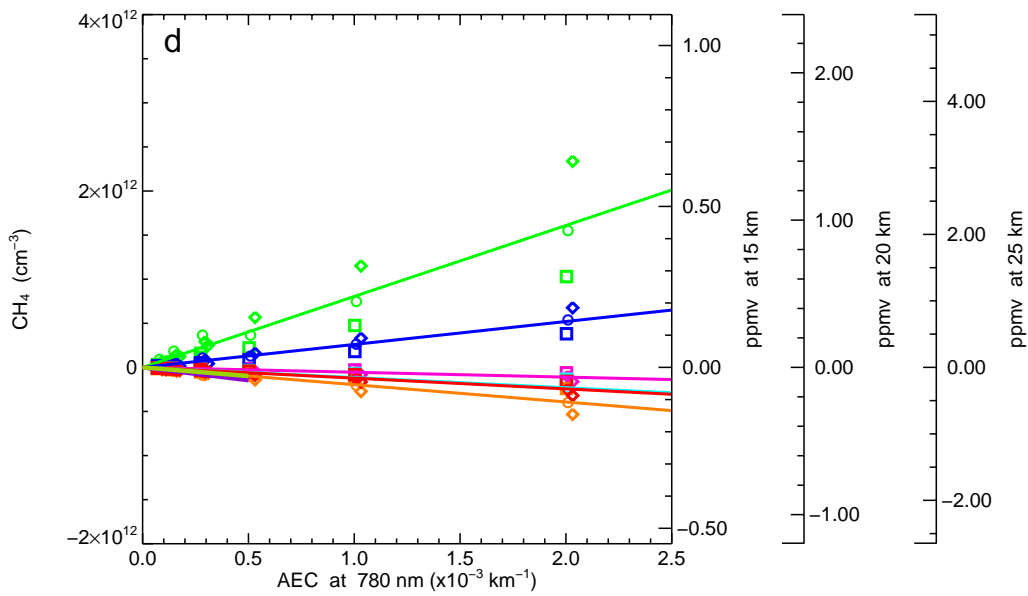
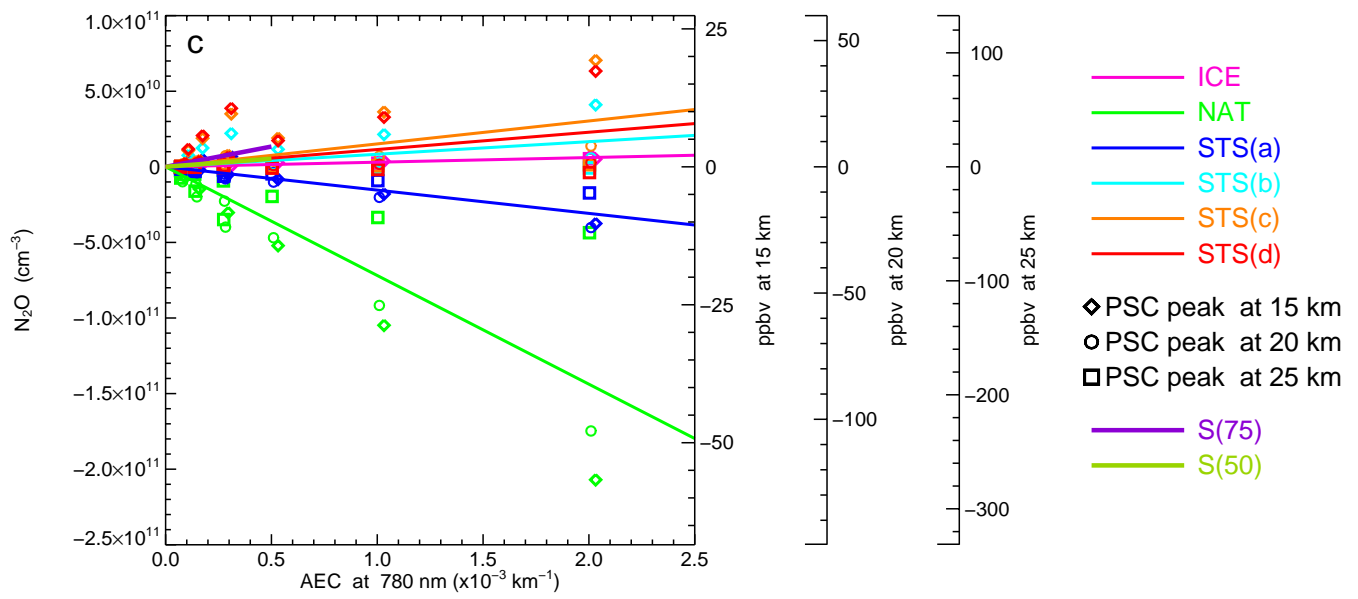


Figure 1 (cont.)

Northern Hemisphere

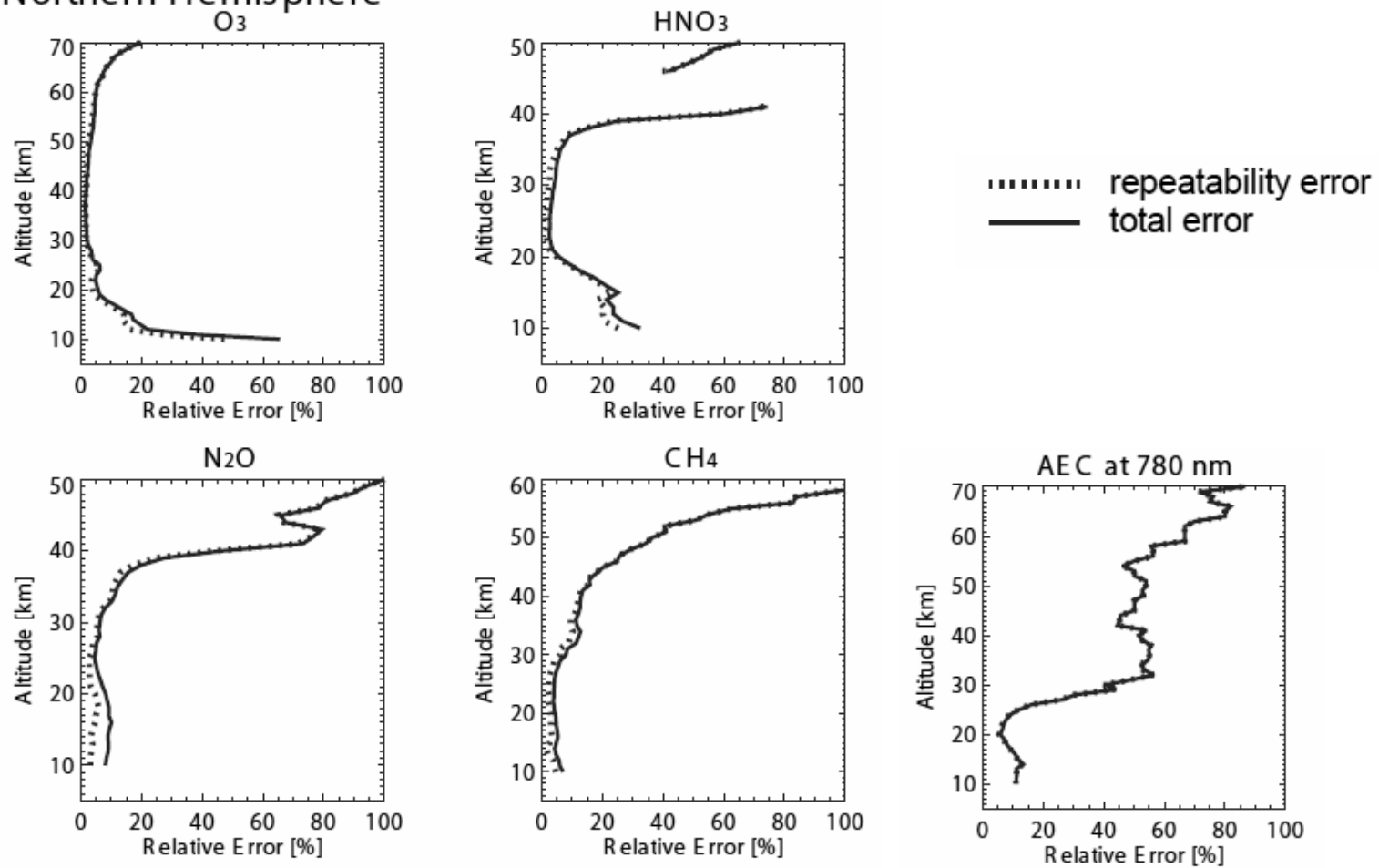


Figure 2

Southern Hemisphere

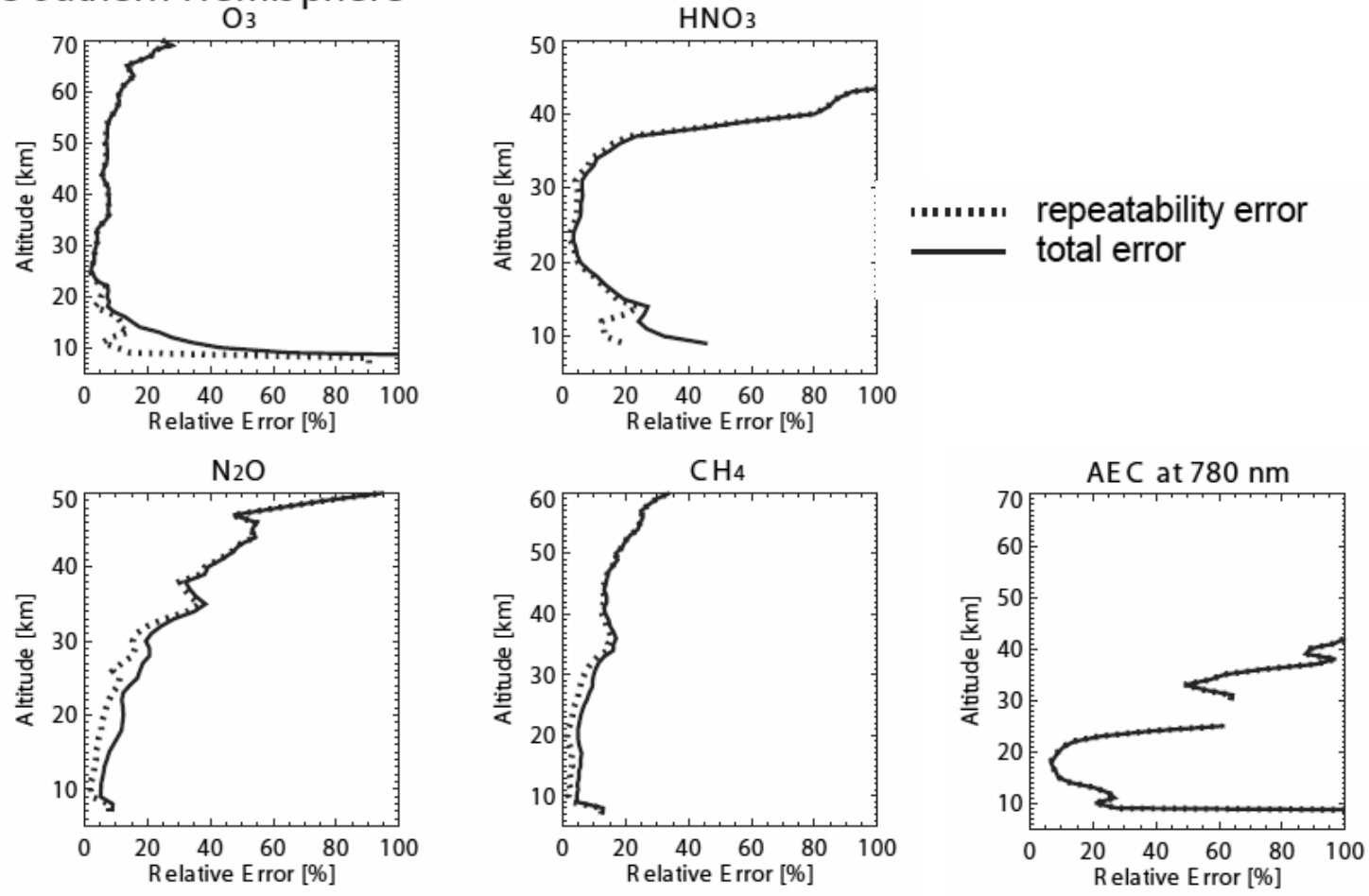


Figure 2 cont.

References:

- Ejiri, M. K., Y. Terao, T. Sugita, H. Nakajima, T. Yokota, G. C. Toon, B. Sen, G. Wetzels, H. Oelhaf, J. Urban, D. Murtagh, H. Irie, N. Saitoh, T. Tanaka, H. Kanzawa, M. Shiotani, S. Aoki, G. Hashida, T. Machida, T. Nakazawa, H. Kobayashi, and Y. Sasano (2006), Validation of the Improved Limb Atmospheric Spectrometer-II (ILAS-II) Version 1.4 nitrous oxide and methane profiles, *J. Geophys. Res.*, 111, doi:10.1029/2005JD006449.
- Griesfeller, A., T. von Clarmann, J. Griesfeller, M. Hoepfner, M. Milz, H. Nakajima, T. Steck, T. Sugita, T. Tanaka, and T. Yokota (2008), Intercomparison of ILAS-II Version 1.4 and Version 2 target parameters with MIPAS-Envisat measurements, *Atmos. Chem. Phys.*, 8, 825-843.
- Irie, H., T. Sugita, H. Nakajima, T. Yokota, H. Oelhaf, G. Wetzels, G. C. Toon, B. Sen, M. L. Santee, Y. Terao, N. Saitoh, M. K. Ejiri, T. Tanaka, Y. Kondo, H. Kanzawa, H. Kobayashi, and Y. Sasano (2006), Validation of stratospheric nitric acid concentration profiles observed by ILAS-II, *J. Geophys. Res.*, 111, doi: 10.1029/2005JD006115.
- Nakajima, H., M. Suzuki, T. Yokota, T. Sugita, Y. Itou, M. Kaji, N. Araki, K. Waragai, H. Yamashita, H. Kanzawa, and Y. Sasano (2002), Tangent height registration for the solar occultation satellite sensor ILAS: A new technique for Version 5.20 products, *J. Geophys. Res.*, 107(D24), 8215, doi:10.1029/2001JD000607.
- Nakajima, H., T. Sugita, T. Yokota, T. Ishigaki, Y. Mogi, N. Araki, K. Waragai, N. Kimura, T. Iwazawa, A. Kuze, J. Tani, H. Kawasaki, M. Horikawa, T. Togami, N. Uemura, H. Kobayashi, and Y. Sasano (2006), Characteristics and performance of the Improved Limb Atmospheric Spectrometer-II (ILAS-II) onboard the ADEOS-II satellite, 111, doi: 10.1029/2005JD006334.
- Nash, E. R., P. A. Newman, J. E. Rosenfield, and M. R. Schoeberl (1996), An objective determination of the polar vortex using Ertel's potential vorticity, *J. Geophys. Res.*, 101, 9471-9478.
- Rothman, L. S., et al. (2005), The HITRAN 2004 Molecular Spectroscopic Database, *HITRAN Special Issue: J. Quant. Spectrosc. Radiat. Transfer*, 96, 139-204.
- Saitoh, N., S. Hayashida, T. Sugita, H. Nakajima, T. Yokota, M. Hayashi, K. Shiraishi, H. Kanzawa, M. K. Ejiri, H. Irie, T. Tanaka, Y. Terao, R. M. Bevilacqua, C. E. Randall, L. W. Thomason, G. Taha, H. Kobayashi, and Y. Sasano (2006), Intercomparison of ILAS-II Version 1.4 aerosol extinction coefficient at 780 nm with SAGE II, SAGE III, and POAM III, *J. Geophys. Res.*, 111, doi: 10.1029/2005JD006315.
- Sasano, Y., T. Yokota, H. Nakajima, T. Sugita, and H. Kanzawa (2001), ILAS-II instrument and data processing system for stratospheric ozone layer monitoring, *Proceedings of SPIE Vol. 4150*, 106-114.
- Sugita, T., H. Nakajima, T. Yokota, H. Kanzawa, H. Gernandt, A. Herber, P. von der Gathen, G. König-Langlo, K. Sato, V. Dorokhov, V. A. Yushkov, Y. Murayama, M. Yamamori, S. Godin-Beekmann, F. Goutail, H. K. Roscoe, T. Deshler, M. Yela, P. Taalas, E. Kyro, S. J. Oltmans, B. J. Johnson, M. Allaart, Z. Litvynska, A. Klekociuk, S. B. Andersen, G. O. Braathen, H. De Backer, C. E. Randall, L. W. Thomason, H. Irie, M. K. Ejiri, N. Saitoh, T. Tanaka, Y. Terao, H. Kobayashi, and Y. Sasano (2006), Ozone profiles in the high-latitude stratosphere and lower mesosphere measured by the Improved Limb Atmospheric Spectrometer (ILAS)-II: Comparison with other satellite-sensors and ozonesondes, *J. Geophys. Res.*, 111, doi: 10.1029/2005JD006439.
- Tanaka, T., H. Nakajima, T. Sugita, M. K. Ejiri, H. Irie, N. Saitoh, Y. Terao, H. Kawasaki, M. Usami, T. Yokota, H. Kobayashi, and Y. Sasano (2007), Tangent height registration method for the Version 1.4 data retrieval algorithm of the solar occultation sensor ILAS-II, *Appl. Opt.*, 46, 7196-7201.

- Wetzel, G., T. Sugita, H. Nakajima, T. Tanaka, T. Yokota, F. Friedl-Vallon, A. Kleinert, G. Maucher, and H. Oelhaf, Intercomparison of ILAS-II version 2 and 1.4 trace species with MIPAS-B measurements, *Atmos. Chem. Phys.*, in press.
- Yokota, T., H. Nakajima, T. Sugita, H. Tsubaki, Y. Itou, M. Kaji, M. Suzuki, H. Kanzawa, J. H. Park, and Y. Sasano (2002), Improved Limb Atmospheric Spectrometer (ILAS) data retrieval algorithm for Version 5.20 gas profile products, *J. Geophys. Res.*, 107, D24, 8216, doi:10.1029/2001JD000628.
- Yokota, T. H. Nakajima, T. Sugita, H. Kawasaki, M. Horikawa, H. Matsuda, N. Uemura, H. Kanzawa, H. Kobayashi, and Y. Sasano (2006), Improved Limb Atmospheric Spectrometer-II (ILAS-II) Version 1.4 algorithm for retrieval of gas and aerosol profiles in the stratosphere (unpublished manuscript).